

Back to the Future: Cycle Encoding Prediction for Self-supervised Contrastive Video Representation Learning

Xinyu Yang
University of Bristol
xinyu.yang@bristol.ac.uk

Majid Mirmehdi
University of Bristol
majid@cs.bris.ac.uk

Tilo Burghardt
University of Bristol
tilo@cs.bris.ac.uk

Abstract

In this paper we show that learning video feature spaces in which temporal cycles are maximally predictable benefits action classification. In particular, we propose a novel learning approach termed Cycle Encoding Prediction (CEP) that is able to effectively represent high-level spatio-temporal structure of unlabelled video content. CEP builds a latent space wherein the concept of closed forward-backward as well as backward-forward temporal loops is approximately preserved. As a self-supervision signal, CEP leverages the bi-directional temporal coherence of the video stream and applies loss functions that encourage both temporal cycle closure as well as contrastive feature separation. Architecturally, the underpinning network structure utilises a single feature encoder for all video snippets, adding two predictive modules that learn temporal forward and backward transitions. We apply our framework for pre-text training of networks for action recognition tasks. We report significantly improved results for the standard datasets UCF101 and HMDB51. Detailed ablation studies support the effectiveness of the proposed components. We publish source code for the CEP components in full with this paper.

1. Introduction

Videos constitute highly structured objects which offer rich and intrinsically correlated information that is often suitable as a self-supervision signal for unsupervised representation learning. Yet, defining which exact aspects of the video should be exploited for effective learning of semantically relevant embeddings, and how the resulting latent spaces are to be constructed, structured, and constrained is a topic of active research [1].

In this paper, we take a closer look at exploiting the bi-directional temporal structure of video to support the learning of semantically relevant high-level spatio-temporal feature spaces. In particular, as illustrated in Figure 1, we show

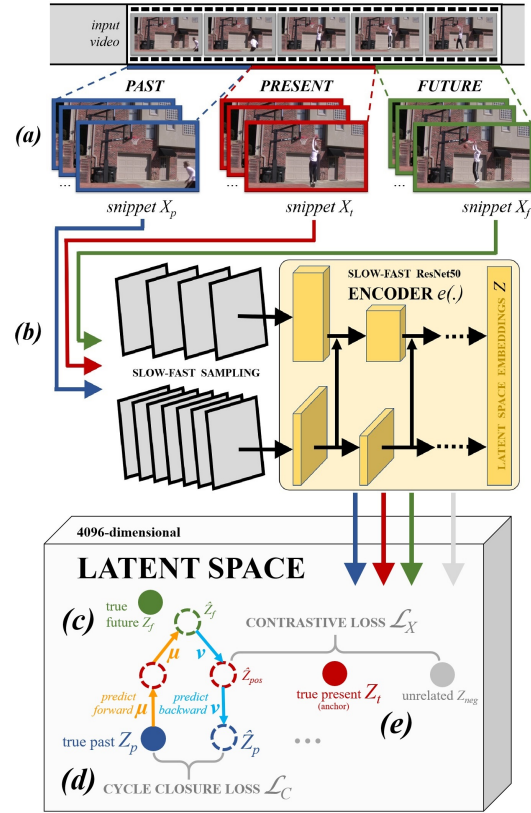


Figure 1. **Overview.** We represent videos in a latent space wherein temporal cycles remain maximally predictable. (a) The raw video data is sampled into snippets where each snippet X_t has a past X_p and future X_f neighbour. (b) In pretext learning, a latent space $Z_t = e(X_t)$ is generated via an encoder network e . (c) In this space, we encourage that learnt temporal forward μ and backward ν predictions form closed cycles (example cycle from past Z_p to some future \hat{Z}_f and back to some past \hat{Z}_p shown). (d) Embedding e and predictors μ and ν are co-trained in a self-supervised manner minimising a loss \mathcal{L}_C that favours cycle closure. (e) Additionally, we apply a contrastive loss \mathcal{L}_X to simultaneously encourage feature separation. We find that this latent space can boost performance in tasks such as action recognition.

that learning spaces, in which temporal cycles (going back and forth in time) become maximally predictable, can benefit action classification. Intuitively, any latent space that is suitable for classifying actions should somehow safeguard the transitive temporal topology which encodes the distinctive ‘playing out’ of actions. Particularly, walking through cycles governed by the temporal axis (*i.e.* progression and later retraction of activity, or vice versa) should cancel out.

Following this idea, we propose a novel pretext learning approach, named Cycle Encoding Prediction (CEP), which operates on unlabelled video and is driven by temporal cycle closure. It aims at constructing a latent embedding wherein loops of temporal forward-backward and backward-forward predictions are structurally preserved and form approximately closed cycles. Meanwhile, similar video states are, as per contrastive learning, still mapped to nearby locations. To generate this space, CEP exploits the bi-directional temporal coherence of video as a self-supervision signal and enforces loss functions that deliver both temporal cycle closure as well as contrastive feature separation. To cope with GPU memory restrictions, we use a memory bank to generate negative features for our contrastive learning. Further, to avoid trivial solutions that are non-semantic-bearing, we introduce inter-batch normalisation as well as exploit clues from optic flow.

It is critical to recognise that the described layout of an embedding space is only ever approximately achievable since video prediction is non-deterministic as illustrated in Figure 2. Given a video snippet (or a corresponding location in embedding space) various possible futures and pasts are feasible. Thus, locations in embedding space that are used for predictions should be treated stochastically only [36].

In summary, our key contributions in this paper are: (i) we present a novel temporal cycle-exploiting minimisation objective for self-supervised pretext learning from unlabelled video that provides superior generalisation and representational ability in latent space, (ii) we introduce the Cycle Encoding Prediction (CEP) approach that implements this minimisation objective in combination with contrastive learning and by adding key components, such as a memory bank and ways to avoid trivial solutions, (iii) we quantitatively compare different self-supervised video representation learning architectures, while different design choices are also investigated to consider the contributions of each component, and (iv) we achieve state-of-the-art performance with significant margins on standard datasets UCF101 and HMDB51. Code and pretrained networks are available at <https://github.com/youshyee/CEP>.

2. Related Work

Self-supervised pretext learning from video, as pursued in this paper, is an unsupervised category of representation learning [11]. Essentially, one has to define an annotation-

free proxy task which demands a network to learn from video-intrinsic information only. Thus, the supervisory signal must exclusively arise from the inherent structure of the raw visual data. Once learned, models can then be utilised as a feature extractor or initialisation for other downstream production tasks.

2.1. Spatial Representation Learning

Still images (or single frames) already provide a wealth of intrinsic spatial and colour channel relationships which form structure and can be utilised for unsupervised learning of the content-specific structure. Tasks such as colourising grey-scale images [16, 38], image inpainting [26], predicting relative image patch positions [3], or image jigsaw puzzles [25, 13] leverage this information. However, whilst single frames can well capture the essence of many high-level semantic concepts such as actions [28] (and self-supervision may be able to learn this information [33]), their expressiveness is limited with regard to many motion-dependent [21] and fine-grained [20] action recognition tasks.

2.2. Spatial-Temporal Representation Learning

Videos contain rich spatio-temporal information that is naturally suitable for unsupervised learning. Many existing works leverage unlabelled videos for spatio-temporal representation learning, such as [33, 23, 17, 12, 8, 37, 5, 34, 18].

Temporal coherence and dynamics of video were exploited for self-supervised learning early in [33]. Positive samples from the tracker, together with the negatives that were sampled randomly, were deployed in a contrastive learning framework with a pre-designed Siamese-triplet network for self-supervised learning.

Alternatively, one may leverage the temporal continuity of video snippets to design the proxy task [23, 17, 35]. Shuffle & Learn [23] discriminates the non-chronologically ordered frames from a video to enforce the learning of temporal relations among frames. Similarly, OPN [17] designs

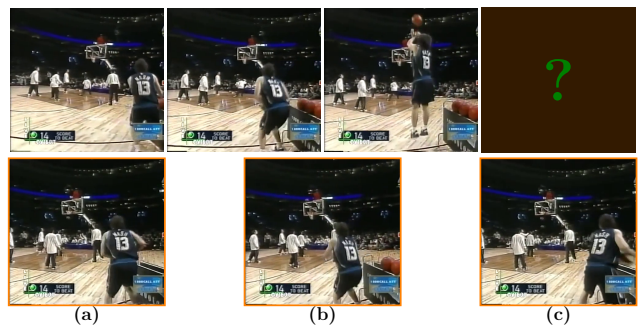


Figure 2. **Ambiguity in Temporal Prediction.** (Top row) Prediction along the temporal axis is clearly non-deterministic, *e.g.* many possible positions of the basketball are feasible given temporally neighbouring video context: (a) score, (b) miss, (c) bounce back.

the learning task by reordering the shuffled frames from a video which enforces the learning of temporal continuity. In VCOP [35], by leveraging the temporal coherence within snippets from a shuffled video, predicting the order becomes the proxy task for self-supervised learning. Rather than sorting whole frames, ST-puzzle [12] focusses on individual non-overlapped spatial patches to introduce a proxy task to re-order permuted 3D spatio-temporal snippets.

Exploring the combination of multi-modalities for spatio-temporal learning is becoming increasingly popular, for example for self-supervised learning. These modalities represent additional metadata, such as captions [22], optical flow [9], audio [14, 27], and so on. Works such as AVTS [14], leverage audio and video correspondence and build a model optimised to discern temporal synchronisation of audio-video pairs to gain a significant boost compared to RGB-only models. More recently, ELO [27] proposed a unified framework for multi-modal and multi-task learning where video together with temporal-aligned audio is utilised. To gain best performance, they apply an evolutionary search algorithm to find the optimal combination of loss functions capturing various tasks and modalities.

Since the introduction of GANs [6], their application towards constructive video generation and prediction have received a great deal of interest. In [32], video frames are partitioned into several spatial regions by different appearance and motion patterns. Exploiting the statistical relationship within the patterns for a known frame can then be used to derive relationships in unknown frames by a dual-stream network. DPC [8] observes an earlier period of a video with a recurrent network for global context extraction. Subsequently, the network makes a prediction for the context of a later period of the video using the Noise Contrastive Estimation (NCE) loss as the constraint for learning. MemDPC [9] extends DPC by appending a memory mechanism that queries a similar pattern from memory when making predictions.

More recently, PRP [37] considers the semantic similarity and temporal structure difference of the same video at different playback rates, introducing multi-task learning objectives that enforce the model to enrich the detail temporally as well as to regress the pre-defined playback rate.

Despite substantial progress in self-supervised learning by prediction, existing methods have not yet fully exploited the representational potential of temporal predictions within video. In this paper, we address this problem by applying a relatively soft set of constraints: the consistency of cyclical temporal predictions and the contrastive separation of features in latent space are the two concepts that drive learning.

3. Cycle Encoding Prediction

We would like to utilise unlabelled video and its property of temporal cycle closure to pretext learn a latent space for

content encoding. To do this, we exploit the bi-directional temporal coherence of video as a self-supervision signal and enforce loss functions that encourage both temporal cycle closure as well as contrastive feature separation. In this section, we describe the overall framework first, and then explore the particular setups and loss functions associated with predicting temporal cycles and contrastive feature separation.

3.1. Framework

CEP operates on video snippets $X_t \in \mathbb{R}^{T \times H \times W \times C}$ harvested from the video stream (as illustrated in Figure 1), where $T \times H \times W \times C$ are, time, height, width, and channel respectively. Given a particular snippet X_t representing the current state, there are two adjacent neighbouring snippets: the past snippet $X_p = X_{t-1}$, and the future snippet $X_f = X_{t+1}$. We consider snippets being encoded within a latent space via a non-linear network $e(\cdot)$, a function which we would like to learn and which should preserve temporal cycle closure as well as contrastive feature separation. Formally, $e(\cdot)$ encodes input video snippets X_t as locations Z_t in latent space, *i.e.*

$$Z_t = e(X_t), \quad (1)$$

where the latent space Z_t is a feature representation of the form \mathbb{R}^D .

On the most fundamental level, we note that if the future state $Z_f = e(X_f)$ or past state $Z_p = e(X_p)$ can be predicted by current Z_t , then the latent space representation must have preserved elementary aspects of the temporal structure of input video clips. To implement this concept, we introduce two predictive functions $\mu(\cdot, \eta)$ and $v(\cdot, \eta)$ to predict future and past states, respectively. We add white noise η in both predictive functions to increase the stochasticity. As it is exemplified in Figure 3, $\mu(\cdot)$ can take past state Z_p and current state Z_t as input and predict the current by the past or predict the future by the current, such that

$$\hat{Z}_f = \mu(Z_t, \eta) = \mu(e(X_t), \eta), \quad (2)$$

$$\hat{Z}_t = \mu(Z_p, \eta) = \mu(e(X_p), \eta). \quad (3)$$

Similarly, the elementary function $v(\cdot)$ allows for the following direct predictions, *i.e.*,

$$\hat{Z}_p = v(Z_t, \eta) = v(e(X_t), \eta), \quad (4)$$

$$\hat{Z}_t = v(Z_f, \eta) = v(e(X_f), \eta). \quad (5)$$

Note that we clearly differentiate between latent space locations Z_t arising directly from the embedding function and \hat{Z}_t arising from predictions solely within latent space.

3.2. Consistency of Predicted Cycles

We observe that the predictive functions can be applied to embeddings recursively, as depicted in Figure 4. Such application allows for the generation of entire cycles of predictions knowing that the future operator $\mu(\cdot)$ is the reverse of the past operator $v(\cdot)$, *i.e.* $\mu(\cdot) = v^{-1}(\cdot)$, or in full detail,

$$Z_t \approx v^{(n)}(\mu^{(n)}(Z_t, \eta), \eta), \quad (6)$$

$$Z_t \approx \mu^{(n)}(v^{(n)}(Z_t, \eta), \eta), \quad (7)$$

where $\mu^{(n)}(\cdot)$ denotes the future predictive function $\mu(\cdot)$ is applied n times.

In contrast to building a loss function directly by measuring the success of predictions (which would require comparison with at least another transfer $e(\cdot)$ into the embedding space), we will instead construct a loss solely *within* the embedding space that encourages closure of cycles. Conceptually, this allows for far greater representational flexibility and generalisation in the latent space whilst still enforcing high-level temporal consistency.

Figure 4 depicts all six basic possible predictive cycles amongst current, future, and past embeddings. Thus, our target is to find a space wherein cycle predictions can be made such as to minimise the distance between the start and end of all closed cycles. Thus, we arrive at the CEP minimisation objective

$$\begin{aligned} \mathcal{L}_C = & \|Z_t - v(\mu(Z_t, \eta), \eta)\|_2 + \|Z_t - \mu(v(Z_t, \eta), \eta)\|_2 \\ & + \sum_{n=1}^2 \|Z_p - v^{(n)}(\mu^{(n)}(Z_p, \eta), \eta)\|_2 \\ & + \sum_{n=1}^2 \|Z_f - \mu^{(n)}(v^{(n)}(Z_f, \eta), \eta)\|_2. \end{aligned} \quad (8)$$

Essentially, this loss sums over the distance errors occurring across the six different basic cycles. Based on this loss, the

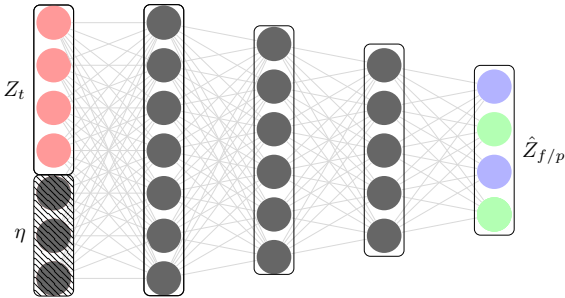


Figure 3. **Structure of the Prediction Functions μ and v .** An embedding Z_t concatenates with white noise η as the input. The two predictors are implemented with 4-layers MLP with Relu activation after each layer. Note that future prediction function and past predictive function share this same architecture, but they do not share parameters in training.

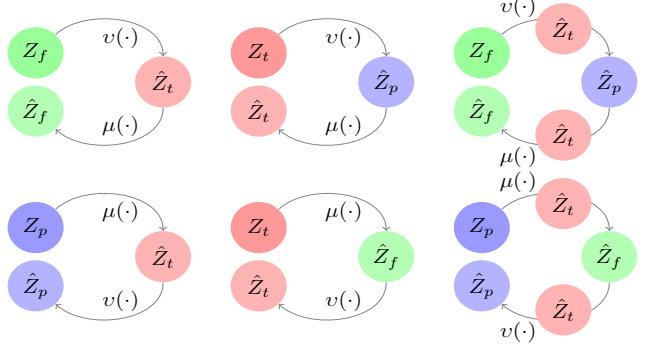


Figure 4. **Elementary Cycles in Embedding Space.** The current, future, and past states are represented in pink, green, and purple respectively. All 6 cycles are considered for cycle consistency. Note that apart from these elementary cycles, the concept could be extended and longer loops are possible, but they require increasing computational resource and a related analysis would be beyond the scope of this paper.

set of parameters θ , that is the union over θ_e for the encoder network together with θ_μ and θ_v , are updated by optimising

$$\arg \min_{\theta} \mathcal{L}_C. \quad (9)$$

Practically to calculate parameters in Eq. 9, the feature encoder and the predictors are co-optimised and evolve together. This process essentially computes an embedding function $e(\cdot)$ that produces a space where closed cycle prediction is maximally achieved. In tandem with this process, both $\mu(\cdot)$ and $v(\cdot)$ are constructed as actual implementations of cycle prediction.

3.3. Contrastive Loss

In addition to encouraging cycle consistency, we would like the elements Z_t of the latent space be organised in such a way that distance separates unrelated features, whilst related ones are situated close by. In order to implement this, we introduce a second loss that enforces contrastive feature separation after performing our predictive tasks. For its implementation, we adopt an extension of the Noise Contrastive Estimation (NCE) approach [7] introduced in [31] and defined as Information NCE (InfoNCE).

In the forward pass, the ground truth representation Z_t and the predicted representation \hat{Z}_t are computed as shown in Figure 1. Z_t is then treated as the anchor, whilst any \hat{Z}_t is treated as a positive sample. Negative samples are taken from mini-batch and memory bank. InfoNCE demands the similarity between the ground truth and positive to be higher than the one between ground truth and negatives. If the similarity is measured by a bi-linear function, a normalised probability P_{pos} can be represented as

$$P_{pos} = \frac{\exp S_p}{\exp S_p + \sum_{i^* \in \mathcal{I}} \exp S_{i^*}}, \quad (10)$$

where $S_p \in \mathbb{R}^1$ denotes the similarity result between the positive pair after the bi-linear operation $S_p = Z_t \cdot \hat{Z}_t^T$, and S_{i^*} represents the results for negative pairs, respectively.

Based on this normalised positive pair distribution P_{pos} , the optimisation task for InfoNCE can be formulated as

$$\arg \min_{\theta} \mathcal{L}_X = -\mathbb{E}_{p \in \mathcal{T}} \left(\log P_{pos} \right). \quad (11)$$

3.4. Memory Bank

Contrastive learning benefits from large mini-batch sizes [10], but given limited GPU memory, it is hard to accommodate both model size and batch size within hardware constraints. Inspired by [10], we increase the cardinality of possible negative samples \mathcal{I} by giving up back-propagation of the gradient for negatives. Instead, we use a proxy encoder $e'(\cdot)$ to generate negative features. The encoder $e'(\cdot)$ is updated based on the encoder $e(\cdot)$, but with momentum,

$$\begin{aligned} \theta_e &\leftarrow \theta_e + \lambda \nabla \mathcal{L} \\ \theta_{e'} &\leftarrow m \theta_{e'} + (1 - m) \theta_e, \end{aligned} \quad (12)$$

where λ is the learning rate for the encoder $e(\cdot)$ and $m \in [0, 1)$ is the momentum coefficient.

As illustrated in Figure 5, \mathcal{I} samples are picked from the memory queue Q during each iteration. Following that, the negative features are generated by proxy encoder $e'(\cdot)$, i.e.

$$Z_{i^*} = e'(X_{i^*}) \mid i^* \in \mathcal{I} \sim Q. \quad (13)$$

3.5. Avoiding Trivial Solutions

Network optimisation is prone to learning the short-cut solutions which circumnavigate the incorporation of semantic-bearing features. Thus, it is essential to formulate the learning task in a way that avoids information leaks.

Batch Normalisation Leaks. As is common practice for training deep neural networks, our encoder $e(\cdot)$ contains Batch Normalisation (BN) layers. However, intra-batch communication among frame snippets may leak information. To resolve this problem, we introduce Inter-Batch Normalisation (IBN) to dilute any leaking signal and perform normalisation across GPUs,

$$y = \gamma \frac{x - \mathbb{E}_{j \sim S} [x_j]}{\sqrt{\text{Var}_{j \sim S} [x_j] + \epsilon}} + \beta, \quad (14)$$

where the mean and standard-deviation is performed on a group of snippets S with the same rank across GPUs, and γ and β are learnable parameters. We demonstrate IBN's effectiveness experimentally in Section 6.

Clue from Optical Flow. A possible trivial solution of CEP could be the generation of temporal predictions from low-level optical flow. To force the model to learn higher-level semantics, the immediately available optical flow signal should be obfuscated. We achieve this by applying

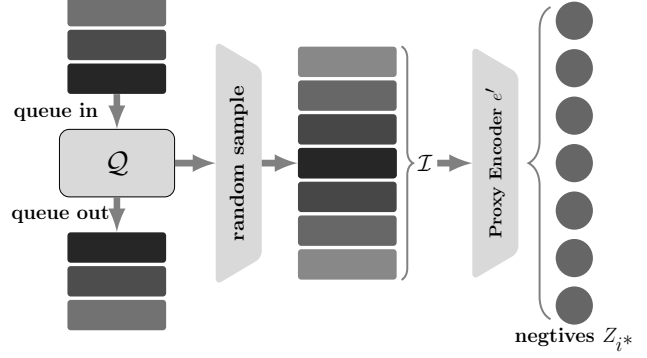


Figure 5. **Memory Bank.** During each training iteration, \mathcal{I} samples are picked from a memory queue Q to stand-in as source material for negative generation. Following that, the negative features are generated by proxy encoder $e'(\cdot)$.

an augmentation strategy to the video snippets, *e.g.* random horizontal flipping, colour jittering, and random cropping. Such snippet-wise augmentation, preserves the temporal coherence within the video snippet signal, whilst the low-level optical flow clue between video snippets is destroyed. We demonstrate the necessity of destroying inter-snippet optical flow experimentally in Section 6.

4. Experimental Setup

Here, we first describe the details of pretext training with CEP, *i.e.* the datasets and environments used for learning. Following that, we evaluate the effect of pretraining on the downstream task of action recognition. We provide detailed ablation studies to support our design decisions.

4.1. Datasets

Kinetics [2] data in its unlabelled form is selected as the initial pre-training dataset. It contains a large body of video comprising 400 action classes, with at least 400 clips for each action. Each video lasts around 10s and is taken from YouTube. The actions are human-focused and range from human-object interactions, such as playing instruments, to human-human interactions, such as shaking hands.

UCF101 [29] is selected as the primary downstream action recognition task for evaluating this work. It contains realistic videos collected from Youtube and involves 101 action categories. UCF101 covers 13K videos with a large variety of different camera motions, object appearances, object poses and scales, as well as background clutter.

HMDB51 [15] is our secondary evaluation dataset and contains 51 action categories in total, covering a wide range of activities from facial actions to body movements. As a popular dataset for action recognition, HMDB51 is sometimes considered more difficult than UCF101 as many classes within the 51 action categories are quite similar.

Method	Year	Dataset	Self-Supervision Training		Modality	Fine-Tuning & Evaluation		
			Resolution	Architecture		Freeze	UCF101	HMDB51
01 — CBT[30]	2019	Kinetics-600	112×112	S3D	RGB	✓	54.0	29.5
02 — CEP		Kinetics-400	112×112	SlowFast	RGB	✓	55.1	31.1
03 — Random Init.	2018	—	112×112	SlowFast	RGB	✗	56.2	23.1
04 — 3D-RotNet[19]		Kinetics-400	112×112	3D-ResNet18	RGB	✗	62.9	33.7
05 — CEP		Kinetics-400	112×112	SlowFast	RGB	✗	68.5	33.4
06 — CEPE		Kinetics-400	112×112	SlowFast	RGB	✗	68.9	34.5
07 — DPC[8]	2019	Kinetics-400	224×224	3D-ResNet34	RGB	✗	75.7	35.7
08 — VCOP[35]	2019	UCF101	224×224	(2+1)D-ResNet	RGB	✗	72.4	30.9
09 — PRP [37]	2020	UCF101	224×224	(2+1)D-ResNet	RGB	✗	72.1	35.0
10 — 3D-Puzzle[12]	2019	Kinetics-400	224×224	3D-ResNet18	RGB	✗	65.8	33.7
11 — CEP		Kinetics-400	224×224	SlowFast	RGB	✗	75.4	36.1
12 — CEPE		Kinetics-400	224×224	SlowFast	RGB	✗	77.0	36.8

Table 1. **Performance Comparison with State-of-the-Art.** The top-1 accuracy rate is reported on downstream action recognition tasks for UCF101 and HMDB51. 'Freeze ✓' represents use of the pretrain model as a feature extractor followed by training on a linear layer to calculate results. 'Freeze ✗' represents end-to-end fine-tuning with the pre-trained model. CEPE represents the CEP model ensemble.

4.2. Implementation Details

Architecture. The non-linear encoding function $e(\cdot)$ is implemented as a ResNet50 SlowFast network [4] with a modified last fully-connected layer yielding an output feature size of 2048. The two predictors v and μ are implemented with 4-layers MLP with Relu activation after each layer, as shown in Figure 3.

Pre-processing. Video snippets X_t of 16 frames each are formed by sampling the original 30fps video at a rate of 6 frames per second. Frames are selected with a consistent stride to preserve the regularity of temporal dynamics. We sample 3 snippets without overlap to form associated triples. For augmentation, we apply snippet-wise random horizontal flip and random colour jittering. Finally, snippets are rescaled and centre-cropped to 224×224 resolution.

Training. We implement the framework in Pytorch version 1.4 using distributed training on 8 GPUs, where each GPU has a mini-batch size of 3 with input tensor sizes being $\mathbb{R}^{3 \times 3 \times 16 \times 224 \times 224}$. As noise function to produce predictor extensions, we use Gaussian noise according to $\eta \in \mathbb{R}^{1024}$. Similar to [24], we use temporal encoder weight shifts with $n = 5000$ for fast convergence while training with Kinetics. For cycle consistency, we run all 6 possible cycles as shown in Figure 4 and use the overall loss \mathcal{L}_C for back-propagation. For contrastive learning, the negative features are sampled from the memory bank with the proxy encoder $e'(\cdot)$ using the momentum coefficient $m = 0.9$. We sample 16 easy negative features from the memory bank, and use 4 hard negative features in the mini-batch where easy negatives are from different videos, whilst the hard negatives are from the same video. The ratio between easy and hard samples is chosen to be 4:1 so as to make the learning task neither too hard to learn nor too easy to overfit. All

the models are trained end-to-end using Stochastic Gradient Decent as optimiser with an initial learning rate of 10^{-2} , momentum 0.9 and weight decay 10^{-4} . The system requires to minimise the combined objective $\mathcal{L} = \lambda \mathcal{L}_C + \mathcal{L}_X$, where λ is set to 0.1 intuitively. During inference, video snippets from the validation set are sampled using the same strategy mentioned above, but all the augmentations are removed maintaining a scaled centre-crop.

Model Ensemble. Since CEP relies on the composition of video snippets as basic blocks of operation, using various models that compose these snippets differently, performance can be further improved. Thus, by integrating different CEP models into a 'panel of expert classifiers' overall model generalisation can be enhanced. As shown in Figure 6, we train an ensemble of CEP classifiers (hereafter referred to as CEPE) where each model follows a different parameterisation. After extensive tests using different hyperparameter combinations for ensemble recruitment, a well performing ensemble model consisting of five CEP models was found: (i) an original CEP setup, (ii) CEP with a $\times 3$ learning schedule, (iii) CEP with a $\times 2$ temporal receptive field, (iv) CEP with a reduced feature space of 2048, and (v) CEP with static memory bank strategy.

5. Results

In this section, we compare CEP's performance by looking at different state-of-the-art self-supervised pretext tasks before fine-tuning on the action classification tasks of UCF101 and HMDB51. At a lower resolution of 112×112 (*i.e.* methods 01–06 in Table 1), we note a significant boost in performance when using straight CEP to 68.5% accuracy on UCF101 and increasing to 68.9% when using the entire CEP model ensemble. To test the generalisability of

the learned CEP feature representation, we also intentionally froze the trained model and trained a linear classifier based on the feature representation defined by the model directly. In comparison with CBT [30] for instance (methods 07–08), CEP better captures the semantics of the video content, achieving 55.1% accuracy on UCF101 and 31.1% on HMDB51. Next, looking at performance when using RGB data at a standard 224×224 resolution (*i.e.* method 07–12). We note that the proposed CEPE approach outperforms all comparable methods, reaching 77.0% and 36.8% accuracy for UCF101 and HMDB51, respectively.

6. Multi-Stream and Ablation Experiments

In this section, we present experiments on an extension to a multi-stream architecture and a detailed ablation study gradually removing components in order to quantify the impact of the CEP concept and its features.

Multi-Stream Architecture - Leveraging additional modalities other than plain RGB in separate network streams often results in a performance boost. AVTS [14], ELO [27], and MemDPC [9] are examples of such multi-stream techniques. By simply adding a second data stream to CEP and CEPE via late fusion, we can start to tap into such an extended information supply. We use two ResNet50 SlowFast streams (one for each modality) and add their 4096-dimensional output in a late fusion fashion. To limit the memory footprint optimisation is performed intermittently every 20 iterations by backpropagating into one stream whilst freezing the other. This extension results in an accuracy of 81.9% for CEPE on UCF101 and 44.1% on HMDB51. To fully explore optical flow and multi-modal performance with CEP, further future work is required to integrate concepts in ELO [27] and MemDPC [9] with the notion of predictive temporal cycle consistency put forward in this paper.

Method	Modality	UCF101	HMDB51
AVTS [14]	RGB+audio	83.7	53.0
ELO [27]	RGB+audio	93.8	67.4
MemDPC [9]	RGB+Flow	86.1	54.5
CEP (dual stream)	RGB+Flow	79.6	42.6
CEPE (dual stream)	RGB+Flow	81.9	44.1

Table 2. **Multi-Modality Study.** Simple duplication of CEP streams for RGB and optical flow does not result in state of the art performance for networks evaluating multiple modality streams. Further work is required to integrate the concepts of MemDPC [9] and ELO [27] with the concepts proposed in this paper.

Architecture and Loss Contributions - For experiments that quantify the influence of removing training with either of the two loss functions, we use a fixed setup of SlowFast with Resnet50 as the encoder. The input is

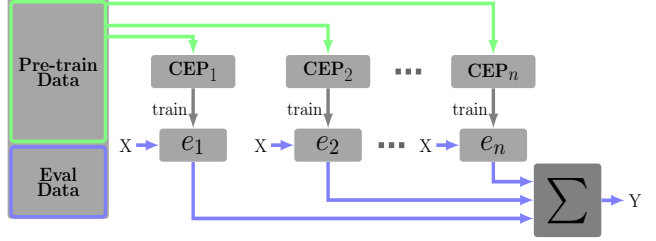


Figure 6. **Model Ensemble.** Our model ensemble consists of several CEP models $\{CEP_1, CEP_2, \dots, CEP_n\}$ with different parameterizations acting together for classification. Individual model decisions are summed over to generate classification decisions.

rescaled and randomly cropped to a resolution of 112×112 . The models are pre-trained on the Kinetics-400 dataset as before, and results are reported after fine-tuning on UCF101 dataset for 30 epochs. As shown in Table 3 all components contribute towards the performance of the CEPE model. The cycle consistency associated loss \mathcal{L}_C in particular, improves accuracy significantly by 4.8%.

Network @ 112×112	Self-Sup. (Kinetics-400) Components	Sup. (UCF) Top1 Acc
SlowFast-Res50	random init.	56.2
SlowFast-Res50	remove \mathcal{L}_X	61.1
SlowFast-Res50	remove \mathcal{L}_C	63.7
SlowFast-Res50	CEP	68.5
SlowFast-Res50	CEPE	68.9

Table 3. **Ablation on CEP Components.** Both \mathcal{L}_X and \mathcal{L}_C can contribute to the performance of CEP. *random init.* means the network does not use any pretext training. *remove \mathcal{L}_C* corresponds to only contrastive learning. *remove \mathcal{L}_X* corresponds to only attaining the consistency of predicted cycles.

Memory Bank Strategies - We quantify the benefit of the memory bank in our framework for a single CEP network operating at a resolution of 224×224 . As shown in Table 4, contrastive learning benefits from a large batch size as demonstrated recently in He *et al.* [10], and feature memory banks can provide this property at controllable cost. We compare two memory bank strategies: (i) static negative features are sampled from the memory bank, and (ii) negatives are generated by a proxy encoder $e'(\cdot)$ dynamically. These models take 4 negatives from the mini-batch and sample 16 negatives from the memory bank per step. We compare these settings against a model without a memory bank that just takes 4 negatives per step from the mini-batch. We conclude that a dynamic memory bank with a large momentum factor can clearly provide benefits to the CEP learning approach.

Feature Space Dimensionality - Table 5 summarises the evaluations on the influence of changing the dimensionality of the embedding space. Unsurprisingly, a larger

Network @224 × 224	Self-Sup. (Kinetics-400)			Sup. (UCF) Top1 Acc
	MemBank	Strategy	m	
SlowFast-Res50	✗	-	-	71.2
SlowFast-Res50	✓	static	-	72.8
SlowFast-Res50	✓	dynamic	0.1	73.3
SlowFast-Res50	✓	dynamic	0.9	75.4

Table 4. **Ablation on Memory Bank Strategies.** It can be seen that a dynamic memory bank with high momentum benefits contrastive learning in CEP. *static* represents a memory bank that saves static features Z_t only; *dynamic* uses a proxy encoder $e'(\cdot)$ to generate negatives dynamically where m represents the momentum coefficient when updating.

Network @224 × 224	Self-Sup. (Kinetics-400)		Sup. (UCF) Top1 Acc
	temp. preserve	output size	
SlowFast-Res50	✓	2 × 2048	73.3
SlowFast-Res50	✗	2048	71.2
SlowFast-Res50	✗	4096	75.4

Table 5. **Ablation on Feature Space Dimensionality.** A large single representational space benefits CEP performance. ✓ represents preserving the temporal dimension for output feature. ✗ means not. Note, CEP with a preserved temporal dimension will have an additional temporal average pooling layer when evaluating.

Network @224 × 224	Self-Sup. (Kinetics-400)		Sup. (UCF) Top1 acc
	time elapsed		
SlowFast-Res50	1.5s		73.7
SlowFast-Res50	3s		75.4

Table 6. **Ablation on the Temporal RF.** A longer temporal receptive field benefits CEP performance. *time elapsed* refers to the clip length as observed by CEP.

representational space benefits performance. Note that for noise η , we use half of the embedding’s feature size, e.g. if $Z_t \in \mathbb{R}^{2048}$ then $\eta \in \mathbb{R}^{1024}$. Splitting the feature space artificially into subspaces to preserve temporal separation was not effective – a single space is advantageous instead.

Temporal Receptive Field - To investigate the effect of the temporal receptive field (RF), we sparsely sample 16 frames as the input. These 16 frames cover either 1.5s or 3s of the input video. As Table 6 show, the input clip with the larger temporal receptive field increases the self-supervised learning performance by 1.7%, which suggests that the model benefits from the scene dynamics for learning the semantics.

Inter-Batch Normalization - Next, we explore the effect of our IBN in preventing the CEP spiralling into a trivial solution. For the BN experiment, the batch size is 3 and for IBN it is 8. The experiment is conducted on 8 GPUs and IBN imposes synchronization and communication between them, so its training takes longer. Table 7 demonstrates the effectiveness of IBN over BN achieving an increase of 3.6%

in self-supervised learning accuracy, proving our hypothesis that short-cut solutions can be mitigated to some extent.

Network @224 × 224	Self-Sup. (Kinetics-400)		Sup. (UCF) Top1 acc
	Norm.		
SlowFast-Res50	BN		71.8
SlowFast-Res50	IBN		75.4

Table 7. **Ablation on Batch Normalization.** IBN implemented in the encoder $e(\cdot)$ can benefit the performance of CEP. IBN is operated on 8 GPUs in distributed training.

Destroying Inter-clip Optical Flow - Finally, we establish that inter-clip optical flow does jeopardize the learning and leads to a trivial solution (see discussion in Section 3.5)) as shown in Table 8.

Network @224 × 224	Self-Sup. (Kinetics-400)		Sup. (UCF) Top1 acc
	preserve inter-opt. flow		
SlowFast-Res50	✓		70.3
SlowFast-Res50	✗		75.4

Table 8. **Ablation on Inter-clip optical flow.** Destroying inter-clip optical flow can prevent CEP being trapped into a trivial solution. ✓ indicates the inter-clip optical flow is preserved by batch-wise data augmentation. ✗ indicates the inter-clip optical flow is destroyed by clip-wise data augmentation.

7. Conclusion

In this paper, we showed that action classification can benefit from learning video feature spaces in which temporal cycles are maximally predictable. We introduced Cycle Encoding Prediction along with associated ensembles (CEP and CEPE) which can effectively encode video in latent spaces wherein the concepts of closed temporal cycles and contrastive feature separation are implemented. The method can be seen as a content-specific regularisation approach used to guide the construction of latent video spaces. It unlocks the related self-supervision signal and is demonstrably effective when used for pretext learning. Ablation studies support the effectiveness of the proposed components. The underpinning network structure only utilises a single feature encoder and two predictive modules that learn temporal forward and backward transitions. When using RGB only we reported significantly improved results for both low and high resolutions for the standard datasets UCF101 and HMDB51. For multi-stream explicit optical flow utilisation further work is required to investigate the utilisation of audio with CEP as well as conceptual integrations of CEP with the key concepts utilised in MemDPC. Future work will also research the enforcement of other properties in latent space in order to unlock a wider range of self-supervision signals from video.

References

- [1] Yoshua Bengio, Aaron Courville, and Pascal Vincent. Representation learning: A review and new perspectives. In *Proceedings of IEEE transactions on pattern analysis and machine intelligence*, pages 1798–1828, 2013.
- [2] Joao Carreira and Andrew Zisserman. Quo vadis, action recognition? a new model and the kinetics dataset. In *CVPR*, pages 6299–6308, 2017.
- [3] Carl Doersch, Abhinav Gupta, and Alexei A Efros. Unsupervised visual representation learning by context prediction. In *ICCV*, pages 1422–1430, 2015.
- [4] Christoph Feichtenhofer, Haoqi Fan, Jitendra Malik, and Kaiming He. Slowfast networks for video recognition. In *ICCV*, pages 6202–6211, 2019.
- [5] Basura Fernando, Hakan Bilen, Efstratios Gavves, and Stephen Gould. Self-supervised video representation learning with odd-one-out networks. In *CVPR*, pages 3636–3645, 2017.
- [6] Ian Goodfellow, Jean Pouget-Abadie, Mehdi Mirza, Bing Xu, David Warde-Farley, Sherjil Ozair, Aaron Courville, and Yoshua Bengio. Generative adversarial nets. In Z. Ghahramani, M. Welling, C. Cortes, N. D. Lawrence, and K. Q. Weinberger, editors, *NeurIPS*, pages 2672–2680. Curran Associates, Inc., 2014.
- [7] Michael Gutmann and Aapo Hyvärinen. Noise-contrastive estimation: A new estimation principle for unnormalized statistical models. In *Proceedings of the Thirteenth International Conference on Artificial Intelligence and Statistics*, pages 297–304, 2010.
- [8] Tengda Han, Weidi Xie, and Andrew Zisserman. Video representation learning by dense predictive coding. In *ICCVW*, pages 0–0, 2019.
- [9] Tengda Han, Weidi Xie, and Andrew Zisserman. Memory-augmented dense predictive coding for video representation learning. In *ECCV*, 2020.
- [10] Kaiming He, Haoqi Fan, Yuxin Wu, Saining Xie, and Ross Girshick. Momentum contrast for unsupervised visual representation learning. In *CVPR*, pages 9729–9738, 2020.
- [11] Longlong Jing and Yingli Tian. Self-supervised visual feature learning with deep neural networks: A survey. *IEEE Transactions on Pattern Analysis and Machine Intelligence*, 2020.
- [12] Dahun Kim, Donghyeon Cho, and In So Kweon. Self-supervised video representation learning with space-time cubic puzzles. In *AAAI*, volume 33, pages 8545–8552, 2019.
- [13] Dahun Kim, Donghyeon Cho, Donggeun Yoo, and In So Kweon. Learning image representations by completing damaged jigsaw puzzles. In *WACV*, pages 793–802. IEEE, 2018.
- [14] Bruno Korbar, Du Tran, and Lorenzo Torresani. Cooperative learning of audio and video models from self-supervised synchronization. In *NeurIPS*, 2018.
- [15] H. Kuehne, H. Jhuang, E. Garrote, T. Poggio, and T. Serre. HMDB: a large video database for human motion recognition. In *ICCV*, 2011.
- [16] Gustav Larsson, Michael Maire, and Gregory Shakhnarovich. Colorization as a proxy task for visual understanding. In *CVPR*, pages 6874–6883, 2017.
- [17] Hsin-Ying Lee, Jia-Bin Huang, Maneesh Singh, and Ming-Hsuan Yang. Unsupervised representation learning by sorting sequences. In *ICCV*, pages 667–676, 2017.
- [18] Xueting Li, Sifei Liu, Shalini De Mello, Xiaolong Wang, Jan Kautz, and Ming-Hsuan Yang. Joint-task self-supervised learning for temporal correspondence. In *NeurIPS*, 2019.
- [19] Jing Longlong and Yingli Tian. Self-supervised spatiotemporal feature learning by video geometric transformations. *arXiv preprint arXiv:1811.11387*, 2019.
- [20] Khoi-Nguyen C Mac, Dhiraj Joshi, Raymond A Yeh, Jinjun Xiong, Rogerio S Feris, and Minh N Do. Learning motion in feature space: Locally-consistent deformable convolution networks for fine-grained action detection. In *ICCV*, pages 6282–6291, 2019.
- [21] Julieta Martinez, Michael J Black, and Javier Romero. On human motion prediction using recurrent neural networks. In *CVPR*, pages 2891–2900, 2017.
- [22] Antoine Miech, Jean-Baptiste Alayrac, Lucas Smaira, Ivan Laptev, Josef Sivic, and Andrew Zisserman. End-to-end learning of visual representations from uncensored instructional videos. In *CVPR*, pages 9879–9889, 2020.
- [23] Ishan Misra, C Lawrence Zitnick, and Martial Hebert. Shuffle and learn: unsupervised learning using temporal order verification. In *ECCV*, pages 527–544. Springer, 2016.
- [24] Volodymyr Mnih, Koray Kavukcuoglu, David Silver, Andrei A Rusu, Joel Veness, Marc G Bellemare, Alex Graves, Martin Riedmiller, Andreas K Fidjeland, Georg Ostrovski, et al. Human-level control through deep reinforcement learning. *nature*, 518(7540):529–533, 2015.
- [25] Mehdi Noroozi and Paolo Favaro. Unsupervised learning of visual representations by solving jigsaw puzzles. In *ECCV*, pages 69–84. Springer, 2016.
- [26] Deepak Pathak, Philipp Krahenbuhl, Jeff Donahue, Trevor Darrell, and Alexei A Efros. Context encoders: Feature learning by inpainting. In *CVPR*, pages 2536–2544, 2016.
- [27] AJ Piergiovanni, Anelia Angelova, and Michael S. Ryoo. Evolving losses for unsupervised video representation learning. In *CVPR*, 2020.
- [28] Karen Simonyan and Andrew Zisserman. Two-stream convolutional networks for action recognition in videos. In *NeurIPS*, pages 568–576, 2014.
- [29] Khurram Soomro, Amir Roshan Zamir, and Mubarak Shah. Ucf101: A dataset of 101 human actions classes from videos in the wild. *arXiv preprint arXiv:1212.0402*, 2012.
- [30] Chen Sun, Fabien Baradel, Kevin Murphy, and Cordelia Schmid. Learning video representations using contrastive bidirectional transformer. *arXiv preprint arXiv:1906.05743*, 2019.
- [31] Aaron van den Oord, Yazhe Li, and Oriol Vinyals. Representation learning with contrastive predictive coding. *arXiv preprint 1807.03748*, 2018.
- [32] Jiangliu Wang, Jianbo Jiao, Linchao Bao, Shengfeng He, Yunhui Liu, and Wei Liu. Self-supervised spatio-temporal representation learning for videos by predicting motion and appearance statistics. In *CVPR*, pages 4006–4015, 2019.
- [33] Xiaolong Wang and Abhinav Gupta. Unsupervised learning of visual representations using videos. In *ICCV*, pages 2794–2802, 2015.

- [34] Xiaolong Wang, Allan Jabri, and Alexei A Efros. Learning correspondence from the cycle-consistency of time. In *CVPR*, pages 2566–2576, 2019.
- [35] Dejing Xu, Jun Xiao, Zhou Zhao, Jian Shao, Di Xie, and Yueting Zhuang. Self-supervised spatiotemporal learning via video clip order prediction. In *CVPR*, 2019.
- [36] Tianfan Xue, Jiajun Wu, Katherine Bouman, and Bill Freeman. Visual dynamics: Probabilistic future frame synthesis via cross convolutional networks. In *NeurIPS*, pages 91–99, 2016.
- [37] Yuan Yao, Chang Liu, Dezhao Luo, Yu Zhou, and Qixiang Ye. Video playback rate perception for self-supervised spatio-temporal representation learning. In *CVPR*, pages 6548–6557, 2020.
- [38] Richard Zhang, Phillip Isola, and Alexei A Efros. Colorful image colorization. In *ECCV*, pages 649–666. Springer, 2016.